

Article

Operando Dual Beam FTIR Study of Hydroxyl Groups and Zn Species over Defective HZSM-5 Zeolite Supported Zinc Catalysts

Long Lin ¹, Xiaotong Zhang ¹ , Ning He ¹, Jiaxu Liu ^{1,*}, Qin Xin ² and Hongchen Guo ¹

¹ State Key Laboratory of Fine Chemicals and School of Chemical Engineering, Dalian University of Technology, No. 2 Linggong Road, Dalian 116024, China; linlong@mail.dlut.edu.cn (L.L.); zhangxiaotong@mail.dlut.edu.cn (X.Z.); heningshixiang@163.com (N.H.); hongchenguo@163.com (H.G.)

² State Key Laboratory of Catalysis, Dalian Institute of Chemical Physics, Chinese Academy of Sciences, Dalian 116023, China; xinqin@dicp.ac.cn

* Correspondence: liujiaxu@dlut.edu.cn; Tel.: +86-411-8498-6162; Fax: +86-411-8498-6162

Received: 30 November 2018; Accepted: 10 January 2019; Published: 17 January 2019



Abstract: A series of defective ZSM-5 zeolites (~300 nm, SiO₂/Al₂O₃ ratio of 55, 100, 480 and 950) were systematically studied by XRD, SEM, ²⁹Si MAS NMR, argon physisorption, NH₃-TPD and FT-IR technologies. The nature, the amount and the accessibility of the acid sites of defective ZSM-5 zeolites are greatly different from reported ZSM-5 zeolites with a perfect crystal structure. The Brønsted acid sites (Si(OH)Al) with strong acid strength and the Brønsted acid sites (hydroxyl nests) with weak acid strength co-existed over defective ZSM-5 zeolites, which leads to a unique catalytic function. Zn(C₂H₅)₂ was grafted onto defective ZSM-5 zeolites through the chemical liquid deposition (CLD) method. Interestingly, FT-IR spectroscopic studies found that Zn(C₂H₅)₂ was preferentially grafted on the hydroxyl nests with weak acid strength rather than the Si(OH)Al groups with strong acid strength over different defective ZSM-5 zeolites. In particular, home-built *operando* dual beam FTIR-MS was applied to study the catalytic performance of Zn species located in different sites of defective ZSM-5 zeolites under real *n*-hexane transformation conditions. Results show that Zn species grafted over hydroxyl nests obtain better dehydrogenative aromatization performance than Zn species over Si(OH)Al groups. This study provides guidance for the rational design of highly efficient alkane dehydrogenative aromatization catalysts.

Keywords: defective ZSM-5; hydroxyl nests; Si(OH)Al; Zn(C₂H₅)₂; chemical liquid deposition; *operando* dual beam FT-IR spectroscopy

1. Introduction

The formation of a “hydroxyl-nest defect” over silica-alumina zeolites, consisting of 4 silanols, a substitute for [AlO₄] tetrahedron, was firstly proposed by Barrer and Makki [1]. After that, Zecchina performed systematically theoretical calculation and found that the hydroxyl nests can be represented as one or more missing [SiO₄] units in the zeolitic framework. In order to preserve the stoichiometry, the obtained microcavities are saturated with neighboring OH groups which are close enough to generate hydroxyl chains interacting through hydrogen bonding [2]. Hydroxyl nests can form during the synthesis of zeolites. The amount of internal defects in zeolites depends conversely upon the concentration of Na and Al impurities [3], while it can be controlled by altering the silica source or changing fluoride as the mineralizing agent [4]. Hydroxyl nests can also form in aluminosilicate or borosilicate zeolite materials by leaching or steaming at high temperatures [5].

Zeolitic material with hydroxyl nests is less hydrophobic than zeolite with an intact structure due to the highly dense presence of internal OH groups [6]. Heitmann et al. found these internal

hydroxyl nests obtain very weak acidity, which is suitable for special applications [7]. For example, Beckman rearrangement reaction (cyclohexanone oxime to form ϵ -caprolactam in gas phase at 350 °C) could be catalyzed by the hydroxyl nests over silicalite-1 with high activity and selectivity [8]. Besides providing weak acidity, the hydroxyl nests could also provide active sites and space for the grafting of heteroatoms such as Sn, Ti and B, etc. [9]. As is well known, the preparation of heteroatom substituted silica-alumina zeolites through direct synthesis occurs at low efficiency, such as in the case of the preparation of Sn-Beta and TS-1 [10,11]. The preparation procedure is usually complex and needs to be controlled strictly. In comparison, grafting heteroatoms over hydroxyl nests by post-treatment could be operated at much milder conditions.

The special property of hydroxyl nests has been known for decades, however, the application of them has only been restricted in the Beckmann rearrangement. Jia et al. reported that the hydroxyl nests are responsible for the rapid deactivation of ZSM-5 zeolite in methanol conversion [12]. The hydroxyl nests accelerate the secondary reaction and coke formation side-reactions [13]. HZSM-5 zeolite with MFI structure (0.55 × 0.55 nm zigzag, 0.55 × 0.57 nm straight channel) [14] has been widely applied in many heterogeneous catalytic processes [15]. The well-developed porous structure with a high surface area and strong acidity endows the extraordinary performance of HZSM-5 as a successful solid acid catalyst. The acidity of HZSM-5 originates from the existence of Si(OH)Al groups. Usually, the Si(OH)Al Brønsted acid sites located at the intersection of the straight channel and zigzag channel of HZSM-5 zeolite obtain the strongest acidity while the Si(OH)Al groups located at other sites obtain slightly weaker acidity. In general, the acid strength of HZSM-5 originating from the Si(OH)Al groups is strong and the attenuation by post-treatment methods such as dealumination and ion-exchange by base metals is widely studied [16,17]. Considering the weak acidity of hydroxyl nests, by regulating the ratio of hydroxyl nests to Si(OH)Al groups, the defective HZSM-5 zeolites with tunable acidity are expected to show novel catalytic properties.

In this study, a series of defective ZSM-5 zeolites with different SiO₂/Al₂O₃ ratio and hydroxyl nests content (~300 nm, SiO₂/Al₂O₃ ratio of 55, 100, 480 and 950) were systematically studied. The Zn modified HZSM-5 zeolites have been extensively studied and testified to be effective in the aromatization of short-chain hydrocarbons [18–20]. Zn(C₂H₅)₂ was grafted onto these defective ZSM-5 zeolites through chemical liquid deposition (CLD) method. We find that Zn(C₂H₅)₂ was preferentially grafted on the hydroxyl nests with weak acidity rather than on the Si(OH)Al groups with strong acidity over different defective ZSM-5 zeolites. The Zn species grafted over hydroxyl nests obtain better dehydrogenation performance than Zn species over Si(OH)Al groups.

2. Result and Discussion

2.1. Defective ZSM-5 Zeolites with Different SiO₂/Al₂O₃ Ratios

The morphology of defective ZSM-5 zeolites with different SiO₂/Al₂O₃ ratios was determined by SEM. As shown in Figure 1, all the crystals of these samples are in a coffin shape and have a homogeneous crystal size of around 300 nm. The XRD patterns of defective ZSM-5 zeolites with different SiO₂/Al₂O₃ ratios are shown in Figure 2. In order to determine the relative crystallinity of these zeolites, the commercial ZSM-5 zeolite (CBV8014 coded as Z80) with SiO₂/Al₂O₃ ratio of 80 was taken as a reference (Figure S1). The typical diffraction peaks of MFI type structure at 7.96, 8.83, 23.18, 23.99 and 24.45° were observed over all of these samples [21]. The Z55 sample obtained the lowest relative crystallinity of 89.84%. In comparison, other defective ZSM-5 zeolites (Z100, Z480 and Z950) obtained similar crystallinity with the commercial Z80 zeolite. For the defective ZSM-5 zeolites, the surface area and pore volume increased with SiO₂/Al₂O₃ ratio (Table 1). Other than Z55, the defective zeolites obtained similar surface area and pore volume to that of Z80 reference (Table S1). These results suggest that the defective ZSM-5 zeolites with high SiO₂/Al₂O₃ ratio are well-crystallized zeolites with similar porous structures of commercial Z80 reference.

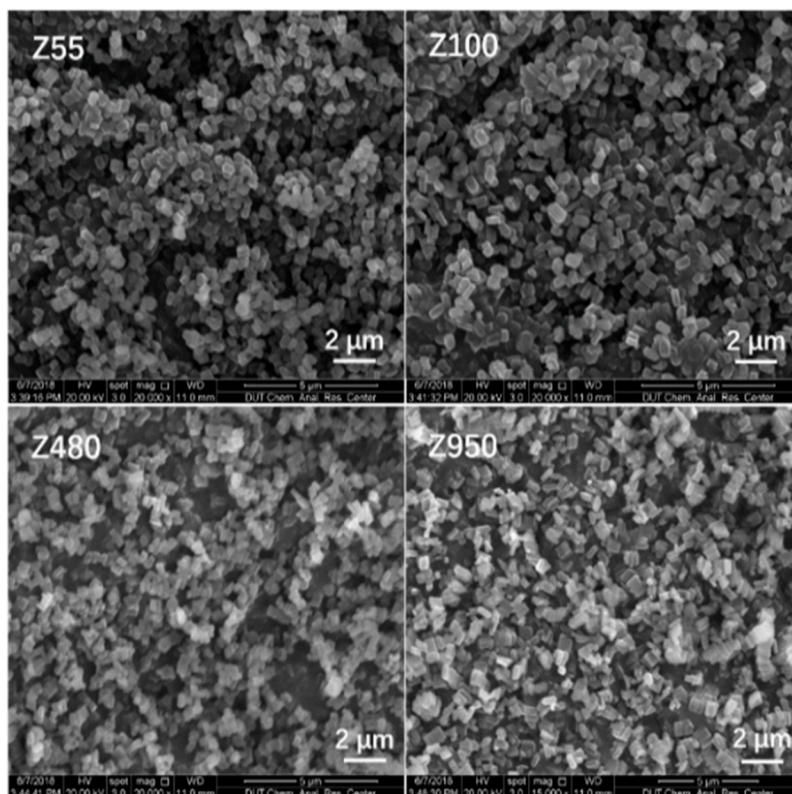


Figure 1. SEM images of defective ZSM-5 zeolites with different $\text{SiO}_2/\text{Al}_2\text{O}_3$ ratios.

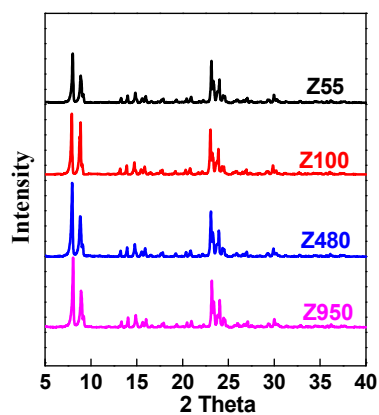


Figure 2. XRD patterns of defective ZSM-5 zeolites with different $\text{SiO}_2/\text{Al}_2\text{O}_3$ ratios.

Table 1. Textural properties of defective ZSM-5 zeolites with different $\text{SiO}_2/\text{Al}_2\text{O}_3$ ratios.

Samples	$\text{SiO}_2/\text{Al}_2\text{O}_3$	S_{BET} (m^2/g)	S_{micro} (m^2/g)	V_{total} (cm^3/g)	V_{micro} (cm^3/g)	Crystallinity (%)
Z55	55	395	362	0.20	0.13	89.84
Z100	100	417	335	0.24	0.13	95.01
Z480	480	437	397	0.23	0.15	98.30
Z950	950	426	382	0.23	0.14	98.31

Note: S_{BET} , BET surface area was calculated by the Brunauer-Emmett-Teller (BET) method; V_{micro} , micropore volume was determined by t-plot; V_{meso} , mesopore volume was determined by $V_{\text{total}}-V_{\text{micro}}$; ZSM-5 zeolite with $\text{SiO}_2/\text{Al}_2\text{O}_3$ ratio of 80 purchased from Zeolyst company (CBV8014) was chosen as reference. The relative crystallinity was estimated by comparing the total XRD peak area of defective ZSM-5 zeolite sample in the range of 2 theta from 22 to 25° with that of the reference ZSM-5.

To our surprise, although the texture properties of the defective ZSM-5 zeolites and Z80 reference are similar, their chemical properties are totally different. The acidity of these samples is characterized by OH-FTIR and NH₃-TPD (Figure 3 and Figure S2). Figure 3a shows the characteristic IR spectra of the defective ZSM-5 zeolites in the range of 3800–3200 cm⁻¹, which corresponds to the OH-stretch vibrations in ZSM-5 zeolites. Three adsorption bands could be identified from the spectra. The band at 3720 cm⁻¹ belongs to the free internal silanol (SiOH) [22]. The band at 3740 cm⁻¹ can be associated with the isolated external silanol (SiOH), and the broad SiOH band centered at around 3500 cm⁻¹ is generally ascribed to hydroxyl nests that consist of a number of silanol groups interacting through extended hydrogen bonding [3,22,23]. The intensity of hydroxyl nests over defective ZSM-5 zeolites is greatly stronger than the other peaks. One thing needs to be paid attention to is that the absorbance of Si(OH)Al groups (3610 cm⁻¹) [22,24] over these zeolites does not show up. These Si(OH)Al groups might be overlapped by hydroxyl nests. Based on these OH-FTIR results, these ZSM-5 zeolites containing substantial amount of hydroxyl nests were defined as defective ZSM-5 zeolites.

The NH₃-TPD profiles of defective ZSM-5 zeolites with different SiO₂/Al₂O₃ ratios are shown in Figure 3b. Generally, the NH₃-TPD profiles of HZSM-5 zeolites have two typical desorption peaks: one centered at about 270 °C (low-temperature peak) and one other at 400 °C (high-temperature peak). The low-temperature peak is associated with acid sites obtaining weak acidity [25–27]. The high-temperature peak is associated with acid sites obtaining strong acidity [28,29]. The total acid amount of these samples decreased gradually with the increasing of the SiO₂/Al₂O₃ ratio. For the Z80 reference, the absorbance of Si(OH)Al groups (3610 cm⁻¹) is greatly stronger than that of the SiOH groups (Figure S2a). The strength and total amount of acid sites over Z80 is considerably larger than that of defective ZSM-5 zeolites (Figure S2b). These differences are possibly caused by the synthesis method of zeolites such as the template applied, crystallization time, silicon and aluminum source.

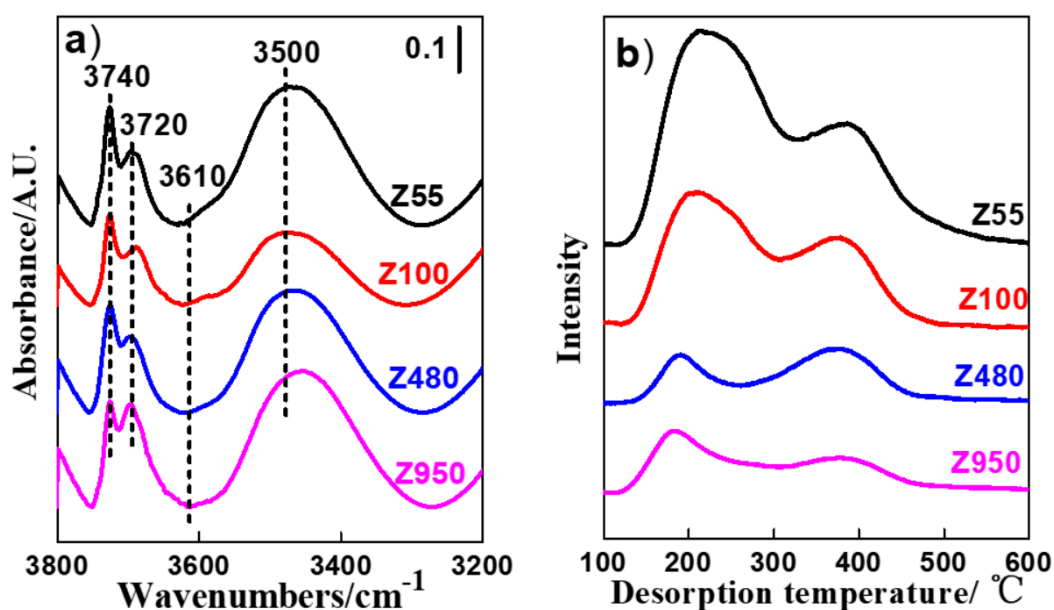


Figure 3. Acidity of defective ZSM-5 zeolites with different SiO₂/Al₂O₃ ratios. (a) FT-IR spectra of hydroxyl groups, (b) NH₃-TPD profiles.

The ²⁹Si MAS NMR spectra of defective zeolites with different SiO₂/Al₂O₃ ratios (Figure 4) show three similar resonances. The strongest resonance at −116 ppm corresponds to Si(OSi)₄ species in the framework of zeolites [30]. The resonance at −106 ppm is assigned to (AlO)₁Si(OSi)₃ species [31] and the resonance at −102 ppm is assigned to (OH)Si(OSi)₃ species [32]. The relative intensity of (AlO)₁Si(OSi)₃ to (OH)Si(OSi)₃ over Z55 is great higher than the other samples which results from its high content of Si(OH)Al groups. For the other defective ZSM-5 zeolites with high SiO₂/Al₂O₃ ratios,

although the OH-FTIR didn't find the Si(OH)Al groups, the Si(OH)Al indeed existed but was greatly influenced by the hydroxyl nests.

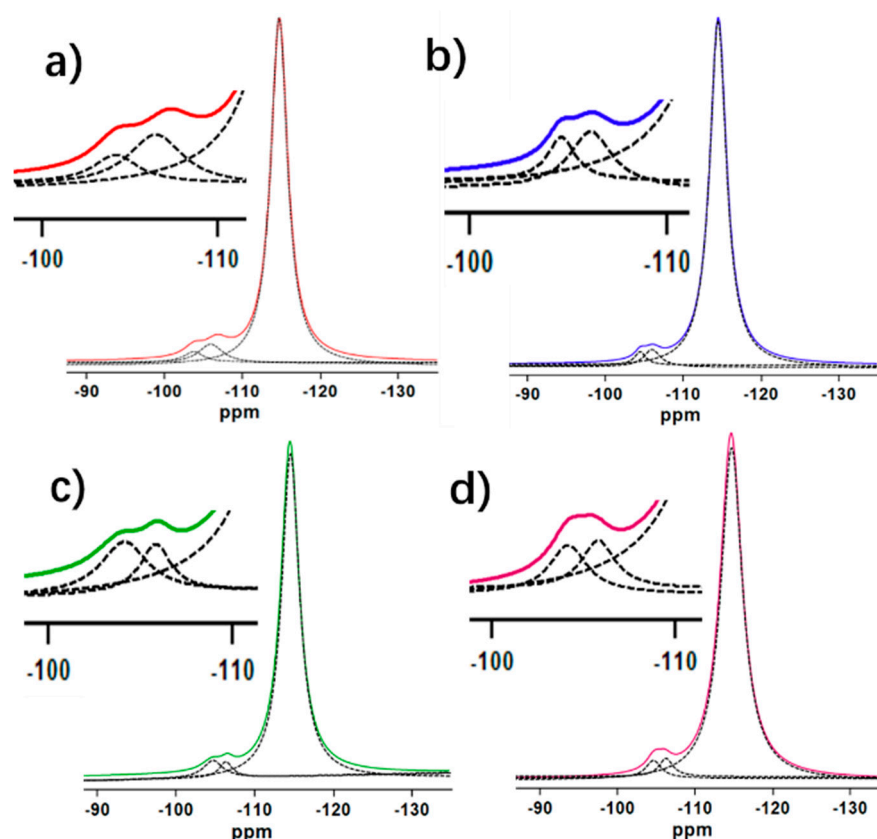


Figure 4. ^{29}Si MAS NMR spectra of defective ZSM-5 zeolites. (a) Z55, (b) Z100, (c) Z480, (d) Z950.

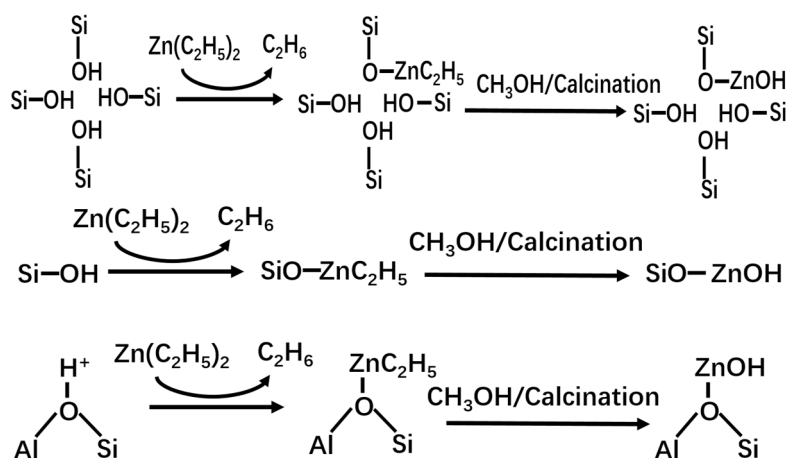
The abovementioned results indicate that these defective ZSM-5 zeolites contain comparable amounts of hydroxyl nests with weak acid strength. The abundant surface OH groups and tunable acidity could endow defective ZSM-5 zeolites novel application.

2.2. Defective HZSM-5 Supported Zn Catalysts Prepared by Chemical Vapor Deposition (CLD) with $\text{Zn}(\text{C}_2\text{H}_5)_2$

In order to explore the potential of defective ZSM-5 zeolites as a working catalyst and disclose the catalytic function of hydroxyl nests, $\text{Zn}(\text{C}_2\text{H}_5)_2$ was grafted onto these defective ZSM-5 zeolites through the CLD method. The interaction between $\text{Zn}(\text{C}_2\text{H}_5)_2$ reactant and hydroxyl groups over zeolites is a stoichiometric reaction [33,34] as shown in Scheme 1. The Zn/Al ratio over Zn grafted different defective ZSM-5 zeolites was controlled at the same level.

OH-FTIR was applied to reveal the relative activity of different hydroxyl groups with $\text{Zn}(\text{C}_2\text{H}_5)_2$ over defective ZSM-5 zeolites. As the results show in Figure 5, for all the defective ZSM-5 zeolites, the $\text{Zn}(\text{C}_2\text{H}_5)_2$ reactant preferentially reacted with the hydroxyl nests (the broad absorbance centered at 3500 cm^{-1}). For Z55, the absorbance of hydroxyl nests of Zn/ZSM-5 gradually decreases with the increasing of the Zn/Al ratio. Meanwhile, the absorbance of internal Si(OH) and external Si(OH) groups at 3720 cm^{-1} and 3740 cm^{-1} , respectively also decrease as the Zn/Al ratio increases. Interestingly, when the absorbance of hydroxyl nests vanishes, the absorbance of the Si(OH)Al at 3610 cm^{-1} shows up. Upon further increasing the Zn/Al ratio, the Si(OH)Al absorbance gradually decreases. These results suggest that the activity of $\text{Zn}(\text{C}_2\text{H}_5)_2$ reacts with different hydroxyl groups following the sequence of hydroxyl nest \geq external SiOH \geq internal SiOH $>$ Si(OH)Al. Similar phenomena have been found over defective ZSM-5 zeolites with high $\text{SiO}_2/\text{Al}_2\text{O}_3$ ratios. Abovementioned results

suggest that Zn species were preferentially grafted on the hydroxyl nests with weak acidity rather than on the Si(OH)Al groups with strong acidity over defective ZSM-5 zeolites. The as-prepared Zn-defective ZSM-5 catalysts might obtain a novel catalytic function.



Scheme 1. The stoichiometric reaction of $\text{Zn}(\text{C}_2\text{H}_5)_2$ modifier and hydroxyl groups over defective ZSM-5 zeolites.

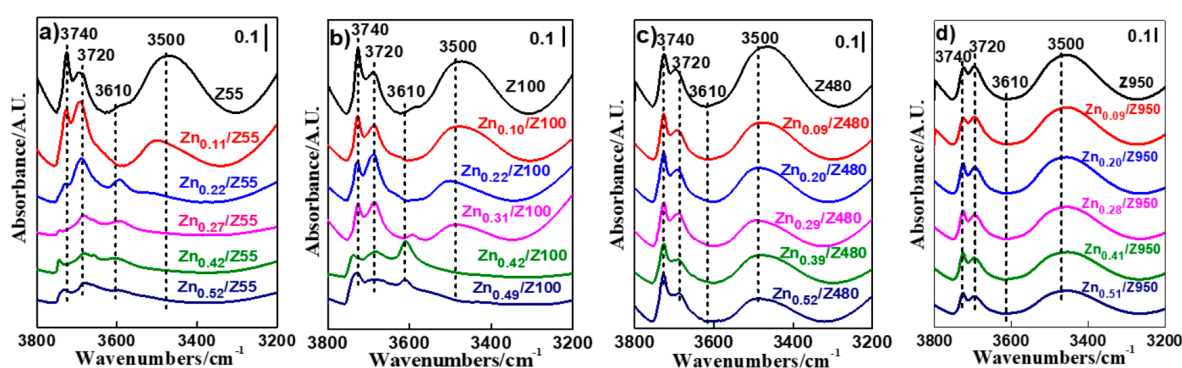


Figure 5. FT-IR spectra of hydroxyl groups on $\text{Zn}(\text{C}_2\text{H}_5)_2$ grafted defective ZSM-5 zeolites with different Zn loading. (a) Zn/Z55, (b) Zn/Z100, (c) Zn/Z480, (d) Zn/Z950.

^{29}Si MAS NMR spectra of Zn modified Z950 zeolites (Figure 6) show that the strongest resonance at -116 ppm corresponding to $\text{Si}(\text{OSi})_4$ species over these samples is at the same level. At the same time, the relative intensity of $(\text{AlO})_1\text{Si}(\text{OSi})_3$ to $(\text{OH})\text{Si}(\text{OSi})_3$ over Z950 increased with the amount of grafted Zn. These results suggest that Zn species was preferentially grafted on the hydroxyl nests over the defective ZSM-5 zeolite with high $\text{SiO}_2/\text{Al}_2\text{O}_3$ ratio.

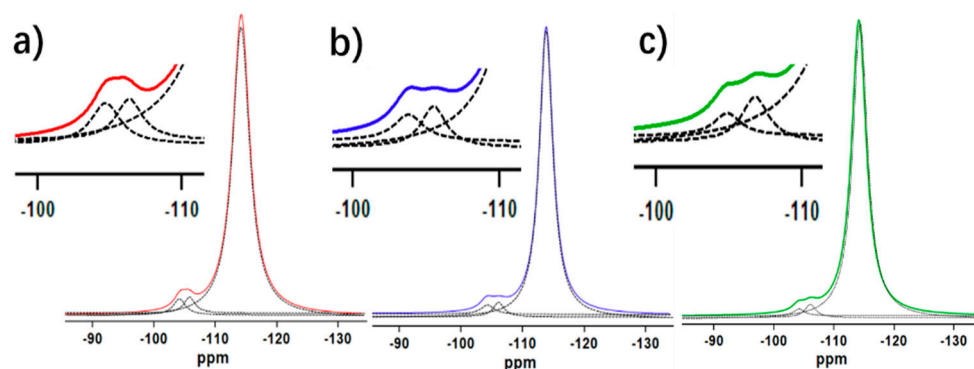


Figure 6. ^{29}Si MAS NMR spectra of Zn modified. (a) Z950, (b) $\text{Zn}_{0.20}/\text{Z950}$, (c) $\text{Zn}_{0.51}/\text{Z950}$ zeolites.

2.3. Properties of Zn Species Located in Hydroxyl Nests Versus in Si(OH)Al

2.3.1. Acid Properties of Zn Species Located in Hydroxyl Nests Versus in Si(OH)Al

The FT-IR and ^{29}Si MAS NMR results show that $\text{Zn}(\text{C}_2\text{H}_5)_2$ preferentially interact with hydroxyl nests on defective ZSM-5 zeolites. In order to selectively graft zinc species on Si(OH)Al groups, eliminating the hydroxyl nests over defective ZSM-5 zeolite is necessary. Defective Z950 zeolite was treated by $(\text{NH}_4)_2\text{SiF}_6$ (AHFS) solutions to prepare a defect-free ZSM-5 zeolite named Z950R [35], then $\text{Zn}(\text{C}_2\text{H}_5)_2$ was grafted onto Z950R. After AHFS treatment, as the OH-FTIR spectra shows in Figure 7, the hydroxyl nests (absorbance centered at around 3500 cm^{-1}) disappeared accompanied the appearance of Si(OH)Al groups (absorbance at 3610 cm^{-1}). These results suggest that the defects of Z950 were largely repaired after AHFS treatment. The Si(OH)Al and SiOH (internal and external) groups are the main active sites of Z950R catalyst. After $\text{Zn}(\text{C}_2\text{H}_5)_2$ grafting, the absorbance at 3610 cm^{-1} corresponding to Si(OH)Al groups gradually decreased until it vanished when the Zn/Al ratio increased to 0.5. However, the absorbance at 3720 and 3740 cm^{-1} corresponding to SiOH groups wasn't clearly influenced. The abovementioned results suggest that most of the Zn species are located in Si(OH)Al groups. Meanwhile, for Zn/Z950 with different Zn loadings, most of the Zn species are located in the hydroxyl nest.

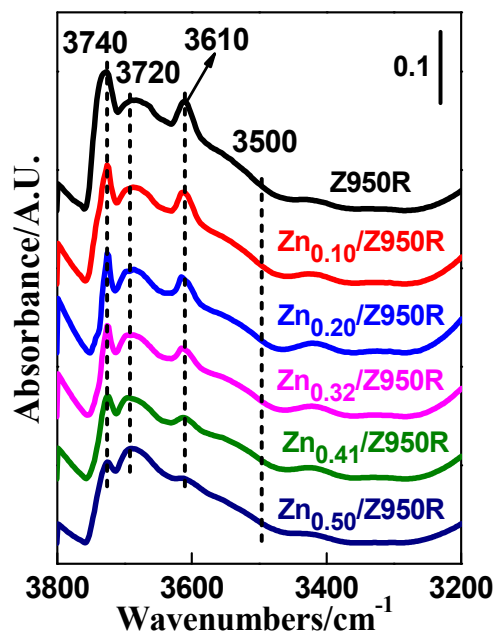


Figure 7. FT-IR spectra of hydroxyl groups on $\text{Zn}(\text{C}_2\text{H}_5)_2$ grafted Z950R zeolite with different Zn loading.

Compared with Z950, after repairing the framework by AHFS, the total amount of acid sites over Z950R obviously increased according to NH_3 -TPD results (Figure 8). Specifically, the amount of acid sites with strong strength increased more obviously. For Z950, after $\text{Zn}(\text{C}_2\text{H}_5)_2$ grafting, the amount of acid sites with medium strength gradually increased while the amount of acid sites with strong strength wasn't obviously influenced. For Z950R, after $\text{Zn}(\text{C}_2\text{H}_5)_2$ grafting, the amount of acid sites with strong strength gradually decreased. While the amount of acid sites with medium strength increased. The reason might lie in the ion exchange reaction between H^+ from Si(OH)Al and Zn species which weakens the acid strength [36]. Abovementioned results also suggest that the Zn species over Z950R and Z950 obtain acidity with medium acid strength.

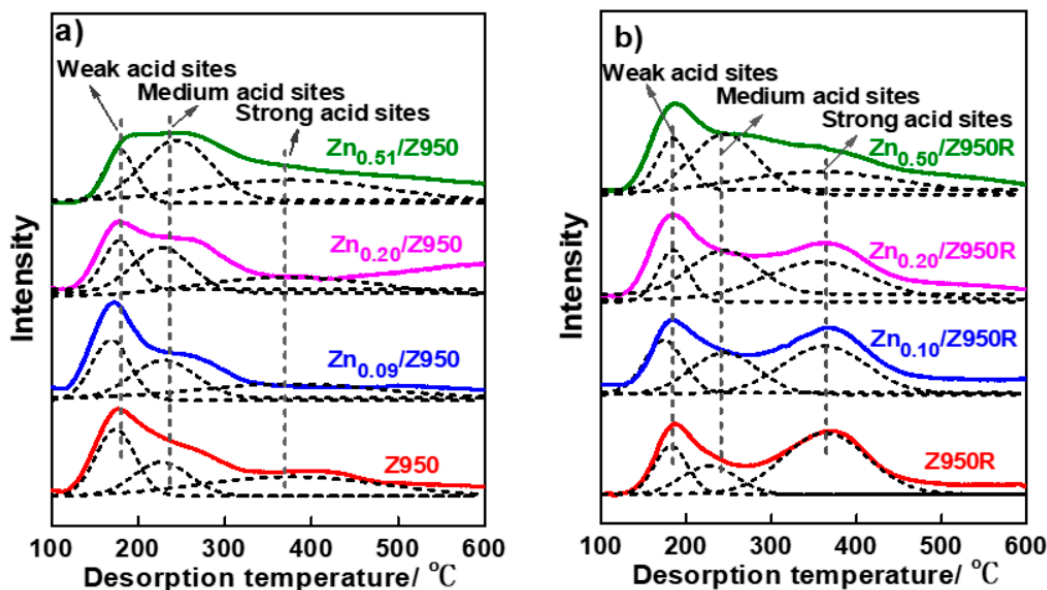


Figure 8. NH_3 -TPD profiles of $\text{Zn}(\text{C}_2\text{H}_5)_2$ grafted over Z950 (a) and Z950R (b) catalysts.

2.3.2. Catalytic Performance of Zn Species Located in Hydroxyl Nests Versus in $\text{Si}(\text{OH})\text{Al}$

The catalytic performance of as-prepared Zn/950 and Zn/950R samples was tested by *n*-hexane transformation using a pulse micro-reactor. The aim is to discriminate the catalytic functions of Zn species located in $\text{Si}(\text{OH})\text{Al}$ groups from hydroxyl nests. The product distributions of *n*-hexane transformation over Zn/Z950 and Zn/Z950R were shown in Figure 9 and Table S2. Based on previous discussions, the Zn modified Z950 catalysts obtain stronger acidity than Zn modified Z950R catalysts. Therefore, the activity of Zn/Z950 in *n*-hexane transformation is greatly higher than that of Zn/Z950R at different temperatures. In order to compare their catalytic performance at the same transformation level, the results of *n*-hexane transformation over Zn/Z950 and Zn/Z950R at 600 °C and 500 °C were chosen, respectively. For Z950, the main products of *n*-hexane transformation are C_2 - C_4 olefins and C_5+ products. The selectivity of benzene, toluene and xylene (BTX) is at a low level. The introduction of Zn significantly increased the activity of *n*-hexane. Moreover, the selectivity of C_2 - C_4 olefins and BTX obviously increased with the Zn loading at the expense of the selectivity of C_1 - C_4 alkanes. For $\text{Zn}_{0.51}/\text{Z950}$, the selectivity of C_2 - C_4 olefins and BTX is 39.03% and 31.13%, respectively. The selectivity of C_1 - C_4 alkanes is only 8.01%, suggesting that Zn species located in hydroxyl nest of defective ZSM-5 zeolite obtain a strong ability to catalyze *n*-hexane dehydrogenative aromatization. The Zn species located in $\text{Si}(\text{OH})\text{Al}$ groups show different performances in *n*-hexane transformation. Although the introduction of Zn into defect-free Z950R zeolite could improve the *n*-hexane activity, the selectivity of BTX only slightly increased. For $\text{Zn}_{0.5}/\text{Z950R}$, the selectivity of C_2 - C_4 olefins and BTX is 34.98% and 13.69%, respectively. The abovementioned results suggest that Zn species locating in $\text{Si}(\text{OH})\text{Al}$ groups of defect-free ZSM-5 zeolite obtain a weaker dehydrogenative aromatization ability.

Operando DB-FTIR-MS was employed to reveal the catalytic functions of Zn species locating in $\text{Si}(\text{OH})\text{Al}$ groups and hydroxyl nests under *n*-hexane reaction conditions [37]. The overall three-dimensional FTIR profiles of *n*-hexane transformation over $\text{Zn}_{0.51}/\text{Z950}$ (a) and $\text{Zn}_{0.50}/\text{Z950R}$ (b) in 180 min are shown in Figure S3. In order to get more detailed information, the selected FT-IR profiles (1300–1700, 2800–3200 and 3200–3800 cm^{-1}) are displayed in Figure 10. For $\text{Zn}_{0.51}/\text{Z950}$ and $\text{Zn}_{0.50}/\text{Z950R}$, as the *n*-hexane absorbance increased, while the hydroxyl group absorbance region (3200–3800 cm^{-1}) wasn't greatly influenced. However, the absorbance of surface C_xH_y species at 1300–1700 and 2800–3200 cm^{-1} obviously increased. Interestingly, a significant absorbance at 1560 cm^{-1} could be seen over $\text{Zn}_{0.51}/\text{Z950}$. This absorbance could most likely be attributed to olefins with internal double bond, polyenic species or precursors of aromatic compounds [38,39]. The effluent

of DB-FTIR cell reactor was monitored by mass spectrometer (Figure 11), $Zn_{0.51}/Z950$ generates a higher amount of olefins and aromatics than $Zn_{0.50}/Z950R$, which indicates that Zn species located in hydroxyl nests obtained better dehydrogenative aromatization performance than Zn species located in $Si(OH)Al$ groups. The reason could be attributed to the accelerated formation of aromatic precursor over Zn species located in hydroxyl nests of defective ZSM-5 zeolite.

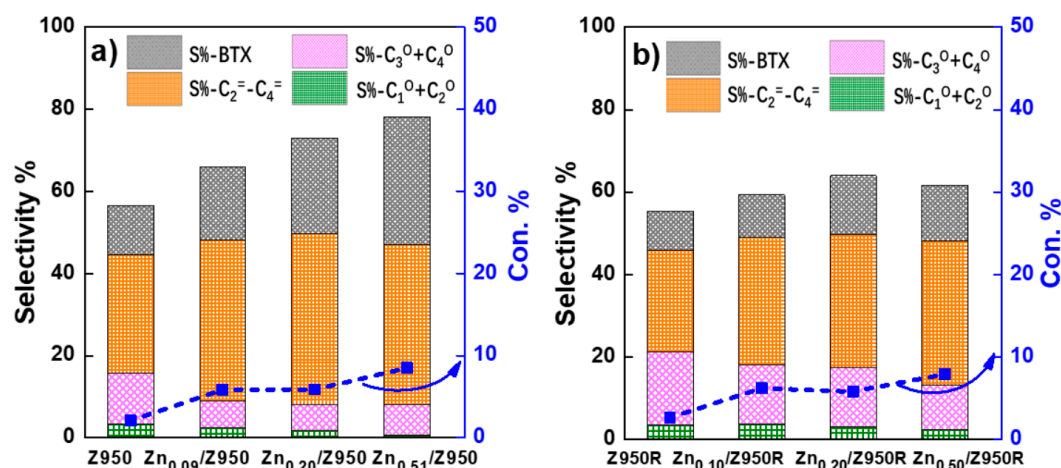


Figure 9. Products selectivity of *n*-hexane aromatization on (a) Zn/Z950 and (b) Zn/Z950R catalysts in pulse micro-reactor. Reaction conditions: T = 600 °C (Zn/Z950) and 500 °C (Zn/Z950R), P = 101.33 kPa.

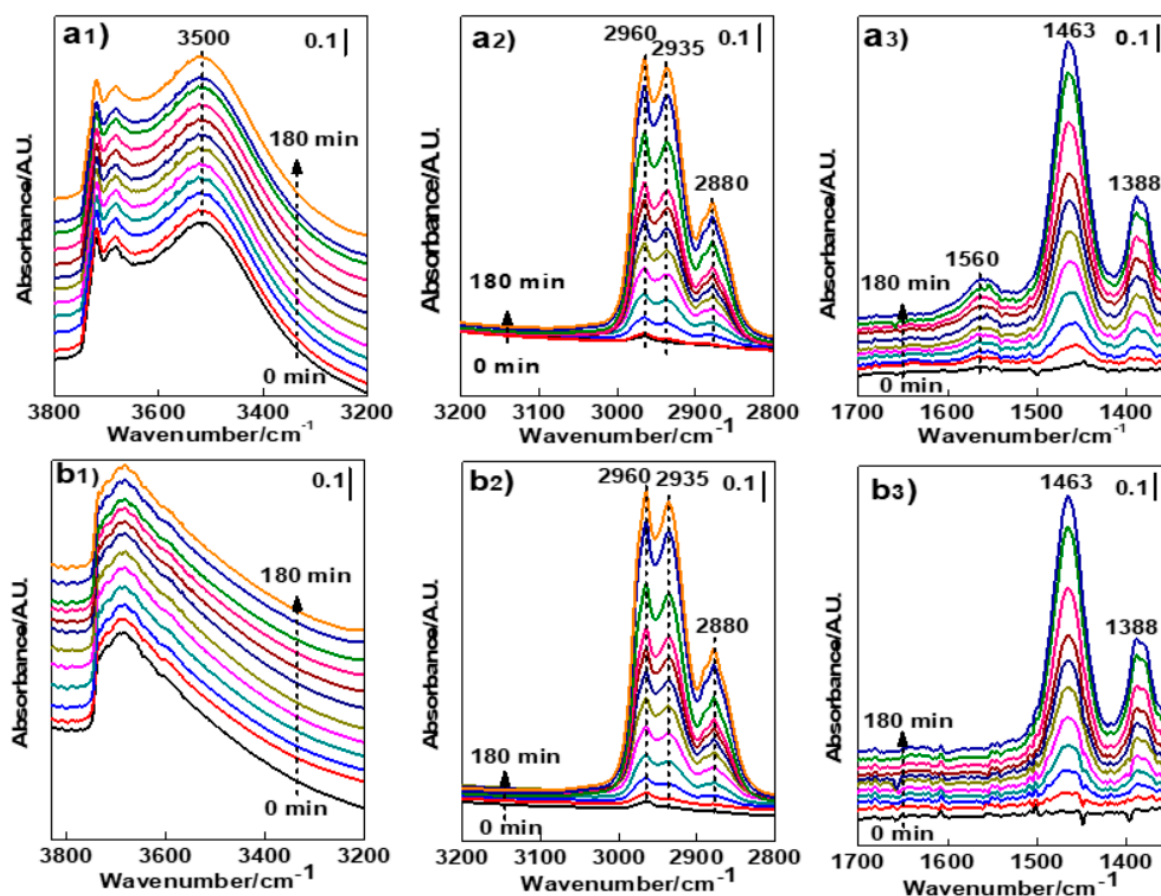


Figure 10. Selected FT-IR profiles of *n*-hexane aromatization over $Zn_{0.51}/Z950$ (a) and $Zn_{0.50}/Z950R$ (b) catalysts obtained over DB-FTIR spectrometer. Reaction conditions: T = 300 °C, P = 101.33 kPa, *n*-hexane was carried into IR-cell reactor by N_2 (10 mL/min), GHSV = 220 h^{-1} .

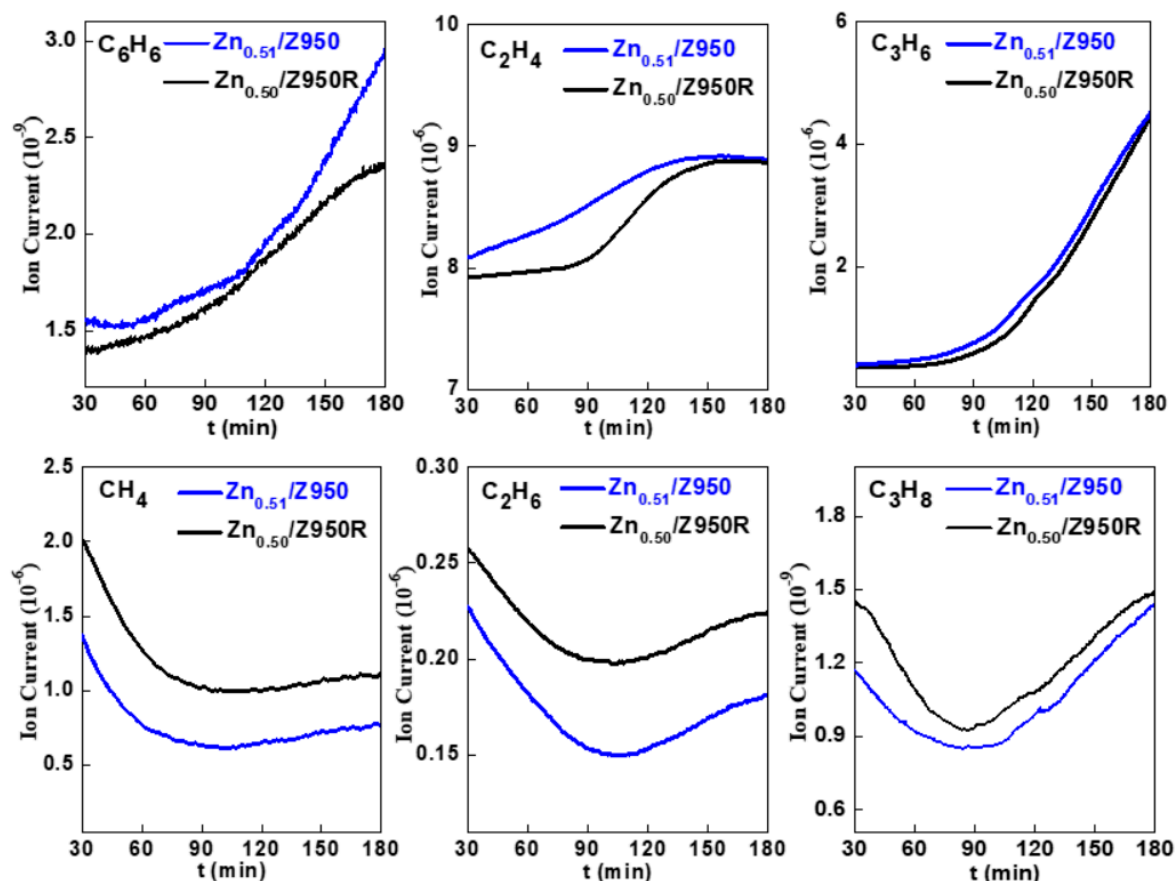


Figure 11. Mass spectra of *n*-hexane aromatization on $Zn_{0.51}/Z950$ and $Zn_{0.50}/Z950R$ catalysts. Reaction conditions: $T = 300\text{ }^{\circ}\text{C}$, $P = 101.33\text{ kPa}$, *n*-hexane was carried into IR-cell reactor by N_2 (10 mL/min), $GHSV = 220\text{ h}^{-1}$.

3. Materials and Methods

3.1. Materials

Nano-sized defective NaZSM-5 zeolite with $\text{SiO}_2/\text{Al}_2\text{O}_3$ molar ratio of 55, 100, 480 and 950 were manufactured by Dalian Ligong Qiwangda Chemical Technology (Dalian, China). The HZSM-5 was obtained by exchanging the NaZSM-5 twice at $80\text{ }^{\circ}\text{C}$ with 1 M solution of NH_4NO_3 with a liquid-to-solid weight ratio of 5 for 1 h. The sample was filtered and washed with deionized water each time after exchange, and finally dried at $110\text{ }^{\circ}\text{C}$ for 12 h and then calcined at $540\text{ }^{\circ}\text{C}$ in flowing dry air for 6 h. The prepared samples were named as Z55, Z100, Z480 and Z950.

Commercial $\text{NH}_4\text{ZSM-5}$ zeolite with $\text{SiO}_2/\text{Al}_2\text{O}_3$ molar ratio of 80 (CBV8014) was purchased from Zeolyst International to compare with the defective ZSM-5 zeolites. The ZSM-5 in hydrogen form was obtained by calcined at $540\text{ }^{\circ}\text{C}$ in flowing dry air for 6 h, named as Z80.

In order to illustrate the catalytic function of defective sites over HZSM-5 in catalysis, the defective sites of ZSM-5 zeolite with $\text{SiO}_2/\text{Al}_2\text{O}_3$ ratio of 950 was repaired by $(\text{NH}_4)_2\text{SiF}_6$ post treatment according to the publicized procedure [35].

3.2. Zn/ZSM-5 Prepared by Chemical Liquid Deposition (CLD) with $\text{Zn}(\text{C}_2\text{H}_5)_2$

Zn was introduced into HZSM-5 by CLD with $\text{Zn}(\text{C}_2\text{H}_5)_2$. All the preparations were performed in a nitrogen-flushed glovebox. An amount of 1 g of dehydrated zeolite (calcination in muffle at $540\text{ }^{\circ}\text{C}$ for 3 h) was suspended in 50 mL of anhydrous *n*-hexane in a 100-mL conical flask with stopper. $\text{Zn}(\text{C}_2\text{H}_5)_2$ (1.0 M solution in *n*-hexane) was slowly added to the mixture via stirring. The mixture was stirred at room temperature for 20 h and centrifuged. The isolated solid was then stirred in 50 mL of

anhydrous methanol for 4 h at room temperature, centrifuged; separated solid was dried at 110 °C for 12 h, and then calcined at 540 °C for 3 h. The resulting zeolite catalysts are designated in the following manner: Zn_X/Y , where X is the practical molar ratio of Zn and Al, Y is the practical SiO_2/Al_2O_3 molar ratios in the catalyst.

3.3. Characterization

The materials were characterized by scanning electron microscopy (SEM); X-ray fluorescence (XRF); inductively coupled plasma optical emission spectrometry (ICP-OES); Argon physisorption; X-ray diffraction (XRD); temperature programmed desorption of NH_3 (NH_3 -TPD); fourier transform infrared spectroscopy (FT-IR) and high resolution ^{29}Si magic angle spinning nuclear magnetic resonance (MAS-NMR).

The scanning electron microscopy (SEM) image used to characterize the surface morphology of the as-prepared zeolite sample was taken on a Quanta 450 scanning electron microscope.

X-ray fluorescence (XRF) measurements (Bruker, Madison, USA) were performed with a Bruker S8 TIGER spectrometer to determine the bulk silicon-to-aluminum ratio.

The molar ratio of Zn and Al was analyzed by inductively coupled plasma optical emission spectrometry (ICP-OES) using an optima 2000DV instrument.

Argon physisorption was conducted on a Micromeritics ASAP 2020 instrument (Micromeritics, Atlanta, USA) at -196 °C to obtain textural information. Prior to the measurement, the samples (380–830 μm sieve fraction) were degassed at 350 °C for 6 h. The surface area was calculated by the Brunauer-Emmett-Teller (BET) method using the adsorption branch in the p/p_0 range from 0.10 to 0.15, and the pore volumes were estimated at p/p_0 of 0.99, while the micro- and mesoporosity was discriminated by the t -plot method.

X-ray diffraction (XRD) patterns were obtained by a Rigaku D/max-2004 diffractometer (Rigaku, Kyoto, Japan) with Cu $K\alpha$ radiation (40 kV, 100 mA) at a $0.02^\circ \text{ min}^{-1}$ (2θ) scanning speed. By assuming that the zeolite sample having the largest peak area in the range of 2θ from 22° to 25° as a reference had a crystallinity of 100% (here it was Z80), the relative crystallinity of each zeolite sample was then estimated by comparing its total peak area in this 2θ range with that of the reference sample.

NH_3 -TPD measurements were carried out in a self-designed flow apparatus using TCD detector (Shimadzu, Kyoto, Japan). Approximately 150 mg of the zeolite sample was used in each measurement, which was first pretreated at 600 °C for 1 h in a helium stream (30 mL/min) and then cooled down to 100 °C. Saturated adsorption of NH_3 on the zeolite sample was then achieved by pulse gaseous NH_3 into the sample tube. After that, the physically adsorbed NH_3 was removed by flushing the sample tube with a helium flow (30 mL/min) at 100 °C for 2 h. To get the NH_3 -TPD profile, the zeolite sample was then heated up from 100 to 600 °C at a ramp of 17° C/min ; the amount of NH_3 released during the heating for desorption was measured by a thermal conductivity detector (TCD).

The spectra of the surface hydroxyl ($-OH$) vibration were obtained with a Nicolet is10 FT-IR spectrometer. The zeolitic samples were pressed into a self-supporting thin wafer (approximately 15 mg) and decontaminated at 400 °C under vacuum (10^{-3} Pa) for 4 h in a quartz IR cell equipped with CaF_2 windows. After the pretreatment, the cell was cooled down to room temperature for the sample measurements. The spectrum was recorded from 4000 to 400 cm^{-1} with an optical resolution of 4 cm^{-1} . The hydroxyl vibration spectra were obtained by subtracting the background spectrum (recorded with an empty IR cell in the absence of sample) from the measured sample spectra.

High resolution ^{29}Si magic angle spinning nuclear magnetic resonance (MAS-NMR) spectra were recorded using an Agilent DD2 500 spectrometer (Agilent Technologies Inc, California, USA).

3.4. Catalytic Tests

3.4.1. Pulse Micro-Reactor

N-hexane conversion tests were performed in a pulse micro-reactor under atmospheric pressure. The catalytic measurements were carried out at 500 and 600 °C respectively. The catalyst sample was pressurized to wafers and then crushed and sieved to 20–40 mesh before use. In a typical run, 200 mg of the zeolite catalyst was loaded, then 1 μ L *n*-hexane was injected into the reactor with the contact reaction time about 0.15 s. The product composition was analyzed by an TECHCOMP GC7900 online gas chromatograph (TECHCOMP, Shanghai, China) equipped with a PLOT-Q column (30 m \times 4 mm) with a flame ionization detector.

The *n*-hexane conversion ($C_{n\text{-hexane}}$) and product selectivity (S_i) were calculated using the following equations:

$$C_{n\text{-hexane}} = (\sum A_i - A_{n\text{-hexane}}) / \sum A_i \times 100\% \quad (1)$$

$$S_i = A_i / (\sum A_i - A_{n\text{-hexane}}) \times 100\% \quad (2)$$

where A_i and $A_{n\text{-hexane}}$ are the corrected chromatographic areas of a specific compound and residual *n*-hexane, respectively.

3.4.2. Home-Built *operando* Dual Beam FTIR-MS

In this case, a self-developed dual beam FT-IR spectrometer, a dual beam IR-cell reactor and an on-line mass spectrometer were used to construct the *operando* spectroscopy system. Catalyst samples were pressed into self-supporting thin wafers (1 cm²) and placed in the sample beam of the dual beam IR cell, and the reference beam was left vacant. The experiment procedures and the method to conduct spectrum subtraction were described elsewhere [22,37,40]. In this study, samples were pretreated in the IR-cell reactor at 400 °C for 4 h under vacuum (10^{−3} Pa). The temperature of *n*-hexane aromatization was carried out at 300 °C. *N*-hexane was carried into IR-cell reactor by nitrogen (10 mL/min), GHSV = 220 h^{−1}. The spectra were recorded at a resolution of 4 cm^{−1} with 64 scans in the region of $\tilde{\nu} = 4000\text{--}400$ cm^{−1}.

During the above FT-IR experiments the changes of the product composition have been monitored by a QMS 200 (Balzers) quadrupole mass-spectrometer. The changes in the signal intensity of the main fragments of benzene, ethylene, propene, methane, ethane, propane and those of the possible products were simultaneously followed.

4. Conclusions

Defective ZSM-5 zeolites with different SiO₂/Al₂O₃ ratios contain a comparable amount of hydroxyl nests with weak acid strength. Unlike defect-free ZSM-5 zeolites, the abundant surface OH groups and tunable acid strength endow defective ZSM-5 zeolites with novel applications.

A FTIR study that found Zn(C₂H₅)₂ was preferentially grafted on the hydroxyl nests with weak acidity rather than Si(OH)Al groups with strong acidity over defective ZSM-5 zeolites with different SiO₂/Al₂O₃ ratios. Zn species located in hydroxyl nests obtained better dehydrogenative aromatization performance than Zn species located in Si(OH)Al groups in *n*-hexane transformation. An *Operando* DB-FTIR-MS study found that Zn species located in hydroxyl nests of defective ZSM-5 zeolite could accelerate the formation of aromatic precursor, resulting in high BTX selectivity.

Supplementary Materials: The following are available online at <http://www.mdpi.com/2073-4344/9/1/100/s1>. Figure S1: XRD patterns of the commercial ZSM-5 zeolite (CBV8014 coded as Z80) and defective Z55 sample; Figure S2: Acidity of Z80 and defective Z55 zeolites. (a) FT-IR spectra of hydroxyl groups, (b) NH₃-TPD profile; Figure S3: The overall three-dimensional FTIR profiles of *n*-hexane aromatization on Zn/Z950 (a) and Zn/Z950R (b) catalysts in 180 min. Reaction conditions: T = 300 °C, P = 101.33 kPa, *n*-hexane was carried into IR-cell reactor by N₂ (10 mL/min), GHSV = 220 h^{−1}; Table S1: Textural properties of Z80 and defective Z55 zeolites; Table S2: Products distribution of *n*-hexane aromatization on Zn/Z950 and Zn/Z950R catalysts in a pulse micro-reactor.

Reaction conditions: T = 500 and 600 °C, P = 101.33 kPa; Scheme S1: Schematic diagram for repairing lattice defects of ZSM-5 zeolite by $(\text{NH}_4)_2\text{SiF}_6$.

Author Contributions: J.X. Liu and H.C. Guo supervised the work; L. Lin, J.X. Liu and H.C. Guo had the idea and designed the experiments, analyzed the results and wrote the manuscript; L. Lin performed the catalyst preparation, characterization and catalytic tests; X.T. Zhang performed the NH_3 -TPD measurement; N. He performed the argon physisorption measurements; Q. Xin supervised the operando DB-FTIR measurements.

Acknowledgments: This work was financially supported by the National Natural Science Foundation of China (21603023) and the Joint Fund Project of NSFC-Liaoning Province (U1508205).

Conflicts of Interest: Author declare no conflict of interest.

References

1. Barrer, R.M.; Makki, M.B. Molecular sieve sorbents from clinoptilolite. *Can. J. Chem.* **1964**, *42*, 1481–1487. [[CrossRef](#)]
2. Zecchina, A.; Bordiga, S.; Spoto, G.; Marchese, L.; Petrini, G.; Leofanti, G.; Padovan, M. Silicalite characterization. Structure, adsorptive capacity, and IR spectroscopy of the framework and hydroxyl modes. *J. Phys. Chem.* **1992**, *96*, 4985–4990. [[CrossRef](#)]
3. Bordiga, S.; Ugliengo, P.; Damina, A.; Lamberti, C.; Spoto, G.; Zecchin, A.; Spano, G.; Buzzoni, R.; Dalloro, L.; Rivetti, F. Hydroxyls nests in defective silicalites and strained structures derived upon dehydroxylation: Vibrational properties and theoretical modelling. *Top. Catal.* **2001**, *15*, 43–52. [[CrossRef](#)]
4. Trzpit, M.; Soulard, M.; Patarin, J.; Desbiens, N.; Cailliez, F.; Boutin, A.; Demachy, I.; Fuchs, A.H. The effect of local defects on water adsorption in silicalite-1 zeolite: a joint experimental and molecular simulation study. *Langmuir* **2007**, *23*, 10131–10139. [[CrossRef](#)] [[PubMed](#)]
5. Deruiter, R.; Kentgens, A.P.M.; Grootendorst, J.; Jansen, J.C.; Vanbekkum, H. Calcination and deboronation of B-MFI single-crystals. *Zeolites* **1993**, *13*, 128–138. [[CrossRef](#)]
6. Heitmann, G.P.; Dahlhoff, G.; Niederer, J.P.M.; Holderich, W.F. Active Sites of a [B]-ZSM-5 zeolite catalyst for the Beckmann rearrangement of cyclohexanone oxime to caprolactam. *J. Catal.* **2000**, *194*, 122–129. [[CrossRef](#)]
7. Heitmann, G.P.; Dahlhoff, G.; Holderich, W.F. Catalytically active sites for the beckmann rearrangement of cyclohexanone oxime to ϵ -caprolactam. *J. Catal.* **1999**, *186*, 12–19. [[CrossRef](#)]
8. Forni, L.; Fornasari, G.; Giordano, G.; Lucarelli, C.; Katovic, A.; Trifiro, E.; Perri, C.; Nagy, J.B. Vapor phase Beckmann rearrangement using high silica zeolite catalyst. *Phys. Chem. Chem. Phys.* **2004**, *6*, 1842–1847. [[CrossRef](#)]
9. Graaff, W.N.P.; Li, G.; Mezari, B.; Pidko, E.A.; Hensen, E.J.M. Synthesis of Sn-Beta with exclusive and high framework Sn content. *Chem. Cat. Chem.* **2015**, *7*, 1152–1160.
10. Corma, A.; Nemeth, L.T.; Renz, M.; Valencia, S. Sn-zeolite beta as a heterogeneous chemoselective catalyst for Baeyer-Villiger oxidations. *Nature* **2001**, *412*, 423–425. [[CrossRef](#)]
11. Corma, A.; Domine, M.E.; Valencia, S. Water-resistant solid Lewis acid catalysts: Meerwein-Ponndorf-Verley and Oppenauer reactions catalyzed by tin-beta zeolite. *J. Catal.* **2003**, *215*, 294–304. [[CrossRef](#)]
12. Jia, Y.M.; Wang, J.W.; Zhang, K.; Liu, S.B.; Chen, G.L.; Yang, Y.F.; Ding, C.M.; Liu, P. Catalytic conversion of methanol to aromatics over nanosized HZSM-5 zeolite modified by $\text{ZnSiF}_6 \cdot 6\text{H}_2\text{O}$. *Catal. Sci. Technol.* **2012**, *7*, 1–3.
13. Bleken, F.L.; Barbera, K.; Bonino, F.; Olsbye, U.; Lillerud, K.P.; Bordiga, S.; Beato, P.; Janssens, T.V.W.; Svelle, S. Catalyst deactivation by coke formation in microporous and desilicated zeolite H-ZSM-5 during the conversion of methanol to hydrocarbons. *J. Catal.* **2013**, *307*, 62–73. [[CrossRef](#)]
14. Kokotailo, G.T.; Lawton, S.L.; Olson, D.H. Structure of synthetic zeolite ZSM-5. *Nature* **1978**, *272*, 437–438. [[CrossRef](#)]
15. Venuto, P.B. Organic catalysis over zeolites: A perspective on reaction paths within micropores. *Microporous. Mater.* **1994**, *2*, 297–411. [[CrossRef](#)]
16. Jin, F.; Cui, Y.G.; Rui, Z.B. Effect of sequential desilication and dealumination on catalytic performance of ZSM-5 catalyst for pyridine and 3-picoline synthesis. *J. Mater. Res.* **2010**, *25*, 272–282. [[CrossRef](#)]
17. Dyballa, M.; Obenaus, U.; Blum, M. Alkali metal ion exchanged ZSM-5 catalysts: On acidity and methanol-to-olefin performance. *Catal. Sci. Technol.* **2018**, *8*, 4440–4449. [[CrossRef](#)]

18. Kazansky, V.B.; Shubbotina, I.R.; Rane, N.; Van Santen, R.A.; Hensen, E.J.M. On two alternative mechanisms of ethane activation over ZSM-5 zeolite modified by Zn²⁺ and Ga¹⁺ cations. *Phys. Chem. Chem. Phys.* **2005**, *7*, 3088–3092. [[CrossRef](#)] [[PubMed](#)]
19. Biscardi, J.A.; Iglesia, E. Non-oxidative reactions of propane on Zn/Na-ZSM5. *Phys. Chem. Chem. Phys.* **1999**, *1*, 5753–5759. [[CrossRef](#)]
20. Penzien, J.; Abraham, A.; van Bokhoven, J.A.; Jentiys, A.; Muller, T.E.; Sievers, C.; Lercher, J.A. Generation and characterization of well-defined Zn²⁺ Lewis acid sites in ion exchanged zeolite BEA. *J. Phys. Chem. B* **2004**, *108*, 4116–4126. [[CrossRef](#)]
21. Zecchina, A.; Bordiga, S.; Spoto, G.; Marchese, L.; Petrini, G.; Leofanti, G.; Radovan, M. Silicalite Characterization. 2. IR spectroscopy of the interaction of CO with internal and external hydroxyl groups. *J. Phys. Chem.* **1992**, *96*, 4991–4997. [[CrossRef](#)]
22. Liu, J.X.; He, N.; Zhou, W.; Lin, L.; Liu, G.D.; Liu, C.Y.; Wang, J.L.; Xin, Q.; Xiong, G.; Guo, H.C. Isobutane aromatization over a complete Lewis acid Zn/HZSM-5 zeolite catalyst: Performance and mechanism. *Catal. Sci. Technol.* **2018**, *8*, 4018–4029. [[CrossRef](#)]
23. Bordiga, S.; Roggero, I.; Ugliengo, P.; Zecchina, A.; Bolis, V.; Artioli, G.; Buzzoni, R.; Marra, G.; Rivetti, F.; Spano, G.; et al. Characterisation of defective silicalites. *J. Chem. Soc. Dalton Trans.* **2000**, *21*, 3921–3929. [[CrossRef](#)]
24. Zecchina, A.; Bordiga, S.; Spoto, G.; Scarano, D.; Petrini, G.; Leofanti, G.; Padovan, M. Low-temperature Fourier-transform infrared investigation of the interaction of CO with nanosized ZSM5 and silicalite. *J. Chem. Soc. Faraday Trans.* **1992**, *88*, 2959–2969. [[CrossRef](#)]
25. Bolis, V.; Busco, C.; Bordiga, S.; Ugliengo, P.; Lamberti, C.; Zecchina, A. Calorimetric and IR spectroscopic study of the interaction of NH₃ with variously prepared defective silicalites: Comparison with ab initio computational data. *Appl. Surf. Sci.* **2002**, *196*, 56–70. [[CrossRef](#)]
26. Li, Y.N.; Liu, S.L.; Xie, S.J.; Xu, L.Y. Promoted metal utilization capacity of alkali-treated zeolite: Preparation of Zn/ZSM-5 and its application in 1-hexene aromatization. *Appl. Catal. A Gen.* **2009**, *360*, 8–16. [[CrossRef](#)]
27. Nishi, K.; Komai, S.; Inagaki, K.; Satsuma, A.; Hattori, T. Structure and catalytic properties of Ga-MFI in propane aromatization. *Appl. Catal. A Gen.* **2002**, *223*, 187–193. [[CrossRef](#)]
28. Choi, S.W.; Kim, W.G.; So, J.S.; Moore, J.S.; Liu, Y.J.; Dixit, R.S.; Pendergast, J.G.; Sievers, C.; Sholl, D.S.; Nair, S.; et al. Propane dehydrogenation catalyzed by gallosilicate MFI zeolites with perturbed acidity. *J. Catal.* **2017**, *345*, 113–123. [[CrossRef](#)]
29. Rodríguez-González, L.; Hermes, F.; Bertmer, M.; Rodríguez-Castellón, E.; Jiménez-López, A. The acid properties of H-ZSM-5 as studied by NH₃-TPD and ²⁷Al-MAS-NMR spectroscopy. *Appl. Catal. A Gen.* **2007**, *328*, 174–182. [[CrossRef](#)]
30. Zhang, J.G.; Qian, W.Z.; Kong, C.Y.; Wei, F. Increasing *para*-xylene selectivity in making aromatics from methanol with a surface-modified Zn/P/Zsm-5 Catalyst. *ACS Catal.* **2015**, *5*, 2982–2988. [[CrossRef](#)]
31. Zhao, J.J.; Zhou, J.; Chen, Y.; He, Q.J.; Ruan, M.L.; Guo, L.M.; Shi, J.L.; Chen, H.R. Fabrication of mesoporous zeolite microspheres by a one-pot dual-functional templating approach. *J. Mater. Chem.* **2009**, *19*, 7614–7616. [[CrossRef](#)]
32. Zhang, W.P.; Bao, X.H.; Guo, X.W.; Wang, X.S. A high-resolution solid-state NMR study on nano-structured HZSM-5 zeolite. *Catal. Lett.* **1999**, *60*, 89–94. [[CrossRef](#)]
33. Almutairi, S.M.T.; Mezari, B.; Magusin, P.C.M.M.; Pidko, E.A.; Hensen, E.J.M. Structure and reactivity of Zn-modified ZSM-5 zeolites: The importance of clustered cationic Zn complexes. *ACS Catal.* **2012**, *2*, 71–83. [[CrossRef](#)]
34. Wang, K.; Cao, G.; Kennedy, G.J.; Afeworki, M.; Bare, R.E.; Hall, R.B. Pore Modification of H-SAPO-34 using dialkyl zinc: Structural characterization and reaction pathway. *J. Phys. Chem. C* **2011**, *115*, 18611–18617. [[CrossRef](#)]
35. Sohn, J.R.; Decanio, S.J.; Fritz, P.O.; Lunsford, J.H. Acid catalysis by dealuminated zeolite Y. 2. The roles of aluminum. *J. Phys. Chem.* **1986**, *90*, 4847–4851. [[CrossRef](#)]
36. Chen, X.H.; Dong, M.; Niu, X.J.; Wang, K.; Chen, G.; Fan, W.B.; Wang, J.G.; Qin, Z.F. Influence of Zn species in HZSM-5 on ethylene aromatization. *Chinese J. Catal.* **2015**, *36*, 880–888. [[CrossRef](#)]
37. Liu, J.X.; Wang, J.L.; Zhou, W.; Miao, C.L.; Xiong, G.; Xin, Q.; Guo, H.C. Construction of an operando dual-beam fourier transform infrared spectrometer and its application in the observation of isobutene reactions over nano-sized HZSM-5 zeolite. *Chin. J. Catal.* **2017**, *38*, 13–19. [[CrossRef](#)]

38. Ivanovaa, I.I.; Kolyagina, Y.G.; Ordonskya, V.V.; Asachenkoa, E.V.; Pasyukovab, E.M. Surface species formed during propane aromatization over Zn/MFI catalyst as determined by in situ spectroscopic techniques. *J. Mol. Catal. A Chem.* **2009**, *305*, 47–53. [[CrossRef](#)]
39. Flego, C.; Peratello, S.; Perego, C.; Sabatino, L.M.F.; Bellussi, G.; Romano, U. Reaction and deactivation study of mesoporous silica-alumina (MSA) in propene oligomerisation. *J. Mol. Catal. A Chem.* **2003**, *581*, 204–205. [[CrossRef](#)]
40. Zhou, W.; Liu, J.X.; Lin, L.; Zhang, X.T.; He, N.; Liu, C.Y.; Guo, H.C. Enhanced dehydrogenative aromatization of propane by incorporating Fe and Pt into Zn/HZSM-5 catalyst. *Ind. Eng. Chem. Res.* **2018**, *57*, 16246–16256. [[CrossRef](#)]



© 2019 by the authors. Licensee MDPI, Basel, Switzerland. This article is an open access article distributed under the terms and conditions of the Creative Commons Attribution (CC BY) license (<http://creativecommons.org/licenses/by/4.0/>).